

Redundancy-Free View Alignment for Multimodal Human Activity Recognition with Arbitrarily Missing Views

Duc-Anh Nguyen[#], Nhien-An Le-Khac⁺

[#] duc-anh.nguyen@ucdconnect.ie, nda97531@proton.me

⁺ an.lekhac@ucd.ie

^{#+} University College Dublin, Ireland

Keywords: multimodal, multiview, missing modality, human activity recognition, contrastive, mixture of experts, redundancy

Abstract

Multimodal multiview learning seeks to integrate information from diverse sources to enhance task performance. Existing approaches often struggle with flexible view configurations, including arbitrary view combinations, numbers of views, and heterogeneous modalities. Focusing on the context of human activity recognition, we propose RALIS, a model that combines multiview contrastive learning with a mixture-of-experts module to support arbitrary view availability during both training and inference. Instead of trying to reconstruct missing views, an adjusted center contrastive loss is used for self-supervised representation learning and view alignment, mitigating the impact of missing views on multiview fusion. This loss formulation allows for the integration of view weights to account for view quality. Additionally, it reduces computational complexity from $O(V^2)$ to $O(V)$, where V is the number of views. To address residual discrepancies not captured by contrastive learning, we employ a mixture-of-experts module with a specialized load balancing strategy, tasked with adapting to arbitrary view combinations. We highlight the geometric relationship among components in our model and how they combine well in the latent space. RALIS is validated on four datasets encompassing inertial and human pose modalities, with the number of views ranging from three to nine, demonstrating its performance and flexibility.

1 Introduction

In multimodal multiview human activity recognition (HAR), parallel data sequences are recorded by sensor units (multiview) of the same or different sensor types (multimodal). The data format depends on sensor types. For instance, at each time step, an accelerometer records a 3D vector $[x, y, z]$, while a camera records a frame or a human pose. Since each sensor has a unique perspective, which is a decisive factor for HAR accuracy [1], sensor fusion can provide more information and enhance accuracy. Early studies on multimodal multiview fusion have proposed to fuse views at the data, feature, or decision

level [2], via concatenation or averaging [3].

Multimodal multiview systems often encounter the view-missing problem, which may arise from device or network failures. Also, sensors may be intentionally omitted during deployment to reduce costs. Relying on any fixed view combination can degrade the task performance when the available views do not align with the system’s original design.

To handle missing views, existing methods often rely on missing-view indicators [4, 5] or reconstruct the missing views using the available ones [6, 7, 8]. However, these approaches supply the model with redundant information because such reconstruction inherently derives from the mutual information among views. In other words, they fill the missing views with information present in the observed views without recovering the underlying information. On the other hand, studies suggest that properly aligning modalities and ensuring coherence among their information can lead to more comprehensive and robust fusion [9]. Multiview contrastive learning pulls different views of the same data sample closer together in the latent space [10]. It is also shown that contrastive learning has a distributional alignment effect [11]. Recent work has integrated contrastive learning into multimodal multiview HAR [12]. Since all sensors observe the same event, they share common information, making this scenario well-suited for contrastive learning, which leverages mutual information to extract robust features across views [13].

In multimodal multiview data, some views may be more informative, while others may contain noise and irrelevant information. Using contrastive learning with these views can degrade high-quality views [14]. For instance, in cycling activity, an accelerometer on the leg is more indicative of the activity than one on the wrist. However, many contrastive learning methods neglect this and treat all views equally. Also, in multiview contrastive learning, the loss function is often computed between every view pair [10], resulting in an $O(V^2)$ time complexity where V is the number of views.

To address the above problems, we propose RALIS (**R**edundancy-free **A**lignment with **C**ontrastive **L**earning and **M**ixture of **E**xperts), which supports arbitrary view combinations during both training and inference. Each view is first processed by a feature extractor, which can be dedicated to that view or shared among homogeneous views. The resulting

features are then combined using an attention-based weighting mechanism. A contrastive loss is used for self-supervised representation learning and to align views, thereby mitigating the impact of missing views on the fusion. This contrastive loss function is trained using the weighted fusion, taking view quality into account. The model head responsible for the main task employs a sparse mixture-of-experts [15] architecture to address the remaining discrepancies among different view combinations. The contributions of this paper are summarized as follows:

- We propose RALIS, a multimodal multiview model capable of handling missing views during both training and inference. It shows that view alignment, without missing view reconstruction or filling, can robustly tackle the view missing problem.
- Our adjusted center contrastive loss mitigates the impact of view missing on the fusion by aligning views in the hyperspherical latent space. It takes view quality into account and reduces time complexity while still being effective.
- A mixture-of-experts module equipped with a specialized load balancing strategy addresses the discrepancies left among different view combinations and generalizes to unseen view combinations.
- We highlight the geometric properties of components in our model, and how they combine well together in a hyperspherical latent space.
- Strong empirical results demonstrate the effectiveness of the proposed method and its robustness to missing views compared to baseline methods.

2 Related Work

2.1 Contrastive Learning

Multiview contrastive learning has proven to be an effective self-supervised representation learning tool. When computing contrastive loss with more than two views, full graph is a typical approach where the loss is computed for all view pairs [16, 17, 18]. In contrast, the core view approach [10] contrasts a core view with other views. It has been shown that full graph performs better as it does not rely on a single core view [19]. For V views, full graph involves $V(V-1)/2$ pairs (i.e., time complexity $O(V^2)$), which increases training time when the number of views is large. COCOA [20] modifies the positive and negative sampling strategy to reduce the number of pairs, thereby lowering time complexity. Alternatively, [21, 22] contrast each view with a concatenation-based view fusion; however, this approach is not flexible to missing views. [23] contrasts individual views with their summation-based fusion, but their adaptive fusion mechanism is restricted to the case of two views and graph-structured data.

To prevent the degradation of high-quality views while contrasting with low-quality ones, [14] assigns a weight to each

pair in the full graph, encouraging more related views to be aligned more strongly. [24] uses maximum mean discrepancy between views to select pairs, encouraging close positives and hard negatives. These methods compute pairwise weights from the feature distributions using discrepancy metrics. In our method, we train the contrastive loss and the main task in a joint learning setting; thus, view weights can be learned from the main task using an attention module.

2.2 Mixture of Experts (MoE)

Recently, sparse MoE [15] has been gaining attention from researchers, especially in the fields of natural language processing and computer vision. Each sparse MoE layer contains a set of sub-networks (experts), and for each input, a gating function activates a subset of specialized experts, enabling conditional computation. Most studies employ it within the Transformer architecture to reduce computation while preserving model capacity, facilitating model scaling [25, 26]. MoE has been used with contrastive learning for feature learning [27] and stabilizing MoE’s gating function [28]. Some studies have applied MoE to multimodal and multiview learning tasks beyond the language-vision domain. For example, it has been used in multiview clustering [29], brain tumor detection [30], Alzheimer’s disease tracking [5], sentiment analysis, and more [4]. Notably, the last two papers leverage MoE in Transformer layers to handle missing modalities, where each expert is specialized in different modality combinations.

2.3 Multimodal Multiview Learning

Missing modality is a common challenge in multimodal multiview systems. In some cases, views may be intentionally omitted during inference to reduce costs. Several studies have addressed this by leveraging multiple views during training and employing a fixed subset of views for inference, using approaches such as co-training with missing modalities [31] and contrastive learning [24, 32]. To offer greater generality and reduce assumptions about available views, many works address arbitrary missing modalities. For example, the model can be trained to reconstruct missing modalities from the available ones [33, 34, 35]. Some studies fill missing data with trainable embeddings, acting as missing data indicators [5, 4]. Another line of work aligns latent distributions among modalities, then imputes missing modalities with the average of the available ones [7]. However, many methods lack full flexibility: some are limited to homogeneous views, others require particular view combinations in the training set.

3 Avoiding Redundant Information Reconstruction

As mentioned in Sections 1 and 2, existing methods often handle missing views by using missing data indicators, which can be learnable embeddings [4, 5] or zero/random values [36]. This approach informs the model which data samples have missing views by filling those missing entries with indicators,

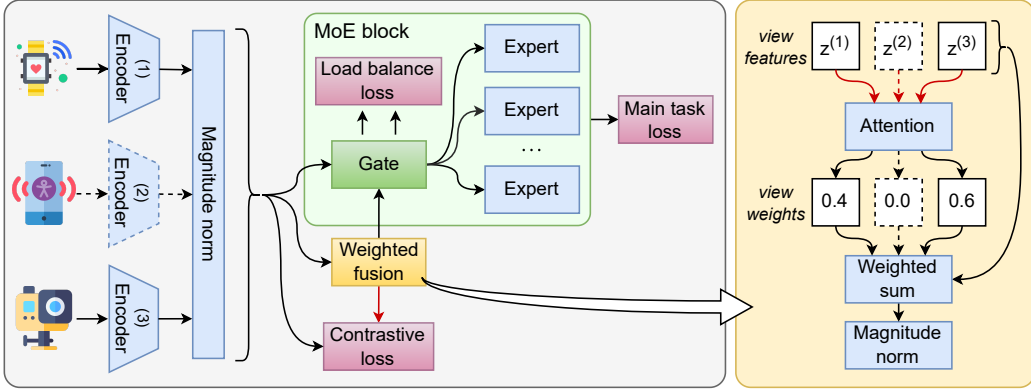


Figure 1: Overview of RALIS. Dashed lines indicate a missing view, which is excluded from computation. Red arrows represent stop-gradient connections, while black arrows allow gradient flow during backpropagation. During inference, the *Weighted fusion* block’s output is the only input to the *MoE* block.

but it does not provide any additional information beyond indicating absence. Many other methods reconstruct the missing views using the available ones [33, 34, 35]. Although this approach seems to recover the missing data, the reconstruction fundamentally depends on the information already present in the observed views. In other words, the reconstructed data inherently derives from the mutual information among views.

From the information theory point of view, when we train a model to reconstruct a missing view C from the observed views A and B , we are trying to minimize the conditional entropy:

$$H(C|A, B) = H(C) - I(C; A, B) \quad (1)$$

where

$$H(C) = - \int p(c) \log p(c) dc \quad (2)$$

is the intrinsic entropy of C determined by its marginal distribution $p(c)$, and is not changed by the reconstruction model. Therefore, the model is essentially learning to maximize the mutual information $I(C; A, B)$. If we directly train the model to maximize this mutual information, it can achieve the same effect without constructing redundant data, thereby reducing workload. Prior studies have shown that multiview contrastive learning can maximize mutual information among views [13, 10], making it suitable for this task.

4 Proposed Method

Suppose we have a training set $\{(x_i^{(v)}, y_i) | i = 1, \dots, N; v = 1, \dots, V\}$, where N is the number of data samples, V is the number of views. The views may correspond to the same or different modalities. The training set may contain missing views and missing labels. We train a model that can operate on any given view combination:

$$\begin{aligned} f_\theta^{(v)} : x^{(v)} &\rightarrow z^{(v)}; v \in \mathcal{S} \\ c_\theta : z^{(\mathcal{S})} &\rightarrow \hat{y} \end{aligned} \quad (3)$$

where f_θ is the encoder, z is the latent vector, \mathcal{S} denotes the set of available views, and c_θ is the model head outputting class logits \hat{y} .

Figure 1 illustrates the RALIS model. The input data from each view is passed through its corresponding encoder to extract feature vectors, which are then normalized to the same magnitude. An attention module assigns a weight to each view within a data sample based on task relevance, enabling view fusion via a weighted sum. The fused vector also goes through magnitude normalization, putting it onto the same hyperspherical feature space as the individual views. During training, both individual and fused representations are passed into the MoE head for classification and are also used for contrastive learning. This ensures the model learns both useful view-specific information and mutual information among views.

All samples, including the unlabeled ones, contribute to the contrastive loss, while only labeled samples train the classifier. At inference time, only the fused representation is input to the classifier. In the following sections, we provide explanations and justifications for the components of the proposed model.

4.1 Adjusted Center Contrastive Loss

Besides the discussion in Section 3, we use contrastive loss in RALIS for two reasons. First, contrastive loss pulls similar data points (positives) together and pushes dissimilar ones (negatives) apart [37]. In this multiview setting, we consider views of the same data sample as positives and views from different samples in a training batch as negatives. Since we fuse views by finding their center in the feature space, the number and distribution of views influence the fusion. By pulling views closer together, contrastive loss improves the fusion’s robustness to view missing (Figure 2).

Second, contrastive learning is widely used for self-supervised representation learning [38, 12]. Even without fusion, studies have shown that multiview contrastive learning can improve uniview models [24, 32].

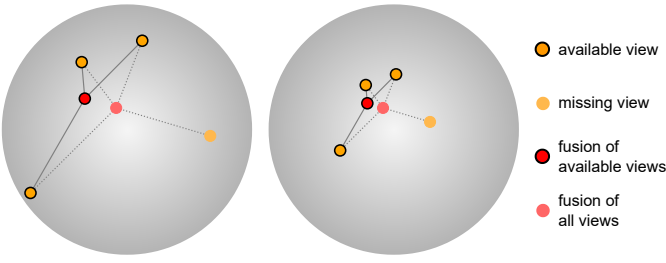


Figure 2: Illustration of fusion robustness to view missing. When views are closer together (right), the fusion shifts less upon view removal than when views are dispersed (left).

4.1.1 Loss Function Definition

For each data sample at index i , the contrastive loss $\mathcal{L}_{\text{pair}}$ between two views a and b is:

$$\ell^{(a,b)} = -\log \frac{g(z_i^{(a)}, z_i^{(b)})}{\sum_j \sum_{v \in \{a,b\}} \mathbb{1}_{[j \neq i \text{ OR } v \neq a]} g(z_i^{(a)}, z_j^{(v)})} \quad (4)$$

$$\mathcal{L}_{\text{pair}}(z^{(a)}, z^{(b)}) = \ell^{(a,b)} + \ell^{(b,a)}$$

where i and j are sample indices within a batch. The function $g(\cdot)$ computes the exponentiated cosine similarity, scaled by a temperature hyperparameter τ :

$$g(z^{(a)}, z^{(b)}) = \exp \left(\frac{z^{(a)} \cdot z^{(b)}}{\|z^{(a)}\| \cdot \|z^{(b)}\|} \cdot \frac{1}{\tau} \right) \quad (5)$$

To compute multiview contrastive loss, the full graph approach contrasts all pairs, pulling all views together (i.e., indirectly pulling all views toward a center). The core view approach contrasts each view with a designated core view, aligning all views toward this core [10]. Full graph often yields better performance than core view, as it does not rely on a single view [19]. However, the core view approach is more efficient, requiring only $V-1$ pairs compared to $V(V-1)/2$ pairs for the full graph. Our method instead aligns all views directly to the center by contrasting each view with the center of the other views (Figure 3). This reduces time complexity while preserving the benefits of the full graph approach. Additionally, view weights can be integrated straightforwardly to adjust the center, enabling control over the influence of individual views with varying quality. Conversely, a full graph approach would require assigning a pairwise weight to every view pair.

As the objective is to pull each view closer to the center, we treat the center as a constant, allowing gradients to flow only through the individual views. Since cosine similarity is used in contrastive loss, vector magnitude can be ignored, and a simple summation places the result vector at the angular center of the constituent vectors. Specifically, our adjusted center contrastive loss is:

$$\mathcal{L}_{\text{AC}} = \frac{1}{V-1} \sum_a^V \underbrace{(1 - w^{(a)})}_{\text{stop grad}} \mathcal{L}_{\text{pair}} \left(z^{(a)}, \underbrace{\sum_{v \neq a}^V w^{(v)} z^{(v)}}_{\text{stop grad}} \right) \quad (6)$$

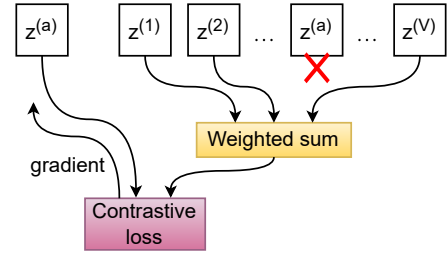


Figure 3: Adjusted center contrastive loss. Each view is contrasted with the other views’ center on the hypersphere.

Listing 1: Python-style pseudocode for adjusted center contrastive loss

```

1  # z: feature vectors of all views [VxNxC]
2  # w: attention weights of all views [VxN]
3
4  num_views, batch, channels = z.shape
5  w = stop_gradient(w)
6  wz = stop_gradient(z * w)
7  center = sum(wz, dimension=0) # [NxC]
8  L = 0
9  for i in range(num_views):
10    zi = z[i] # [NxC]
11    c = center - wz[i]
12    L += contrast_pair(zi, c) * (1 - w[i])
13 return L / (num_views - 1)

```

The weight term $w(v)$ puts the center closer to higher-quality views, causing all views to be pulled more toward those of higher quality. The term $1-w^{(a)}$ acts as a loss weight, assigning a lower weight when the loss function tries to pull a high-quality view (i.e., when $w(a)$ is large) toward others. This weight will be discussed in Section 4.2. The loss term is divided by $V-1$ instead of V to compensate for the scale decrease caused by the weight $1-w^{(a)}$. Specifically, the total scaling factor is:

$$\frac{\sum_a^V (1 - w^{(a)})}{V - 1} = \frac{V - \sum_a^V w^{(a)}}{V - 1} = \frac{V - 1}{V - 1} = 1 \quad (7)$$

So Equation (6) is a weighted average of $\mathcal{L}_{\text{pair}}$ across views.

4.1.2 Loss Function Implementation

Listing 1 demonstrates how \mathcal{L}_{AC} in Equation (6) is implemented. The function *contrast_pair* is the contrastive loss between a pair of views $\mathcal{L}_{\text{pair}}$ defined in Equation (4). In this implementation, we compute $\sum_v^V w^{(v)} z^{(v)} - w^{(a)} z^{(a)}$ instead of $\sum_{v \neq a}^V w^{(v)} z^{(v)}$ as in Equation (6). Although they produce identical results, the former avoids re-computing the fusion every iteration, i.e., $O(V^2N)$. It computes the fusion once and subtracts each individual view from that fusion in the loop, i.e., $O(VN+VN)$. Including the *contrast_pair* function, the total time complexity of Listing 1 is $O(VN+V(N^2+N))$, which simplifies to $O(VN^2)$.

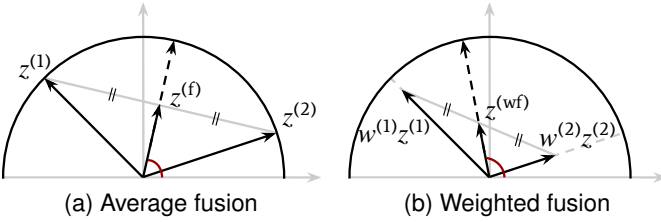


Figure 4: Fusion of two vectors. The fused vector $z^{(wf)}$ is oriented more toward the vector with a higher weight.

The full graph approach, which considers all possible view pairs, has a complexity of $O(V^2N^2)$. COCOA [20] reduces this by removing cross-view negative pairs, resulting in $O(V^2N+VN^2)$. In contrast, our method combines views rather than removing them, achieving $O(VN^2)$. Any multi-view contrastive loss function has a minimum time complexity of $O(N^2)$, as this is required for computing a single view pair. Assuming that the number of data samples N is fixed across methods, we focus on the dependency on V . Without considering N , our approach improves the time complexity from $O(V^2)$ to $O(V)$.

4.2 Attention-based View Fusion

We employ an attention module to capture differences in data quality and task relevance among views. Fusion is performed via a weighted sum followed by vector magnitude normalization. As a result, the fusion lies in the center of the individual views, while being closer to high-quality views on the hypersphere (Figure 4). This not only improves the fusion for the main task, but also alleviates the degradation of high-quality views when contrasted with low-quality ones using the adjusted center contrastive loss.

Following prior work [39, 40, 41], we process each view independently without explicitly modeling cross-view interactions. This design naturally accommodates missing views without missing data indicators or reconstruction. Also, because it processes views separately, it is not affected by unseen view combinations.

Specifically, we use a shared MLP network containing two fully connected layers and a ReLU activation in between to compute a scalar weight for each view, and a softmax function to normalize view weights. We stop the backward gradient flow between the encoders and the attention module (Figure 1) to ensure only the attention module learns view importance, while the encoders focus exclusively on feature extraction. View weights are computed as follows:

$$w^{(v)} = \text{softmax}(\text{MLP}(\underbrace{z}_{\text{stop grad}}))_v \quad (8)$$

Then, the weighted fusion is:

$$z^{(wf)} = \sum_v^V w^{(v)} z^{(v)} \quad (9)$$

This fused representation is used for both classification and contrastive loss. Since the view attention module is trained with the main task’s loss function, it learns view importance specific to the main task.

4.3 Mixture of Expert Classifiers

We use a MoE for the classification head to further process residual discrepancies among view combinations not captured by the contrastive loss. Each expert in the MoE specializes in handling different patterns, and the gating mechanism routes inputs to the most suitable experts.

The previous sections demonstrate that individual views are pivotal in the fusion process, especially with missing views. Therefore, we train the classification head using both the fused representation and each individual view. While contrastive learning captures mutual information across views, training on individual views extracts useful view-specific features. Also, since the fusion lies at the center of the individual views, this training approach strengthens the robustness to arbitrary, unseen view combinations.

Because the fusion and individual views are trained for different purposes, we design a load balancing strategy that separates them, preventing the individual views from occupying part of the expert pool.

4.3.1 MoE Head

We adopt the sparse MoE architecture with a noisy top-K gating network [15], where each input token is processed by K experts. Other studies often use MoE in conjunction with the Transformer architecture [5, 4], modeling cross-view interaction. Because our model processes views separately, we integrate MoE without the self-attention layer commonly seen in Transformer. Each expert is an MLP network outputting class logits. The MoE classification head is:

$$\hat{y} = \sum_e^E \text{Gate}(z, K)_e \text{Expert}_e(z) \quad (10)$$

For each input z of an individual view or the fusion, the gate outputs a set of weights across the E experts. Only the top K experts are kept and their weights are passed into a softmax function, while the rest are assigned a weight of 0.

Finally, since our main task is classification, the cross-entropy loss function H is used:

$$\mathcal{L}_{\text{cls}} = \frac{1}{V+1} \left(H(y, \hat{y}^{(wf)}) + \sum_v^V H(y, \hat{y}^{(v)}) \right) \quad (11)$$

4.3.2 Load Balancing

The load balancing loss encourages the gate to distribute input tokens more evenly among the experts, preventing expert overuse or underuse. As we train individual views and the fusion together, combinations with only one view are trained much more than any other combinations that may appear in the

fusion. Consequently, the whole set of tokens is encouraged to spread evenly, but one-view and multi-view combinations may be allocated to disjoint sets of experts. If this happens, it will nullify the purpose of training individual views to strengthen the model’s robustness to unseen view combinations.

To address this, we compute the load balancing loss below for the individual views and the fusion separately, promoting both to spread evenly across experts.

$$\mathcal{L}_{LB} = CV^2(\{importance_e\}_e^E) + CV^2(\{load_e\}_e^E) \quad (12)$$

The *importance* for each expert quantifies the total gating weight assigned to that expert across tokens; the *load* measures how many tokens are dispatched to each expert, indicating the actual token count; CV^2 is the coefficient of variation squared function $CV^2(x) = (\sigma(x)/\mu(x))^2$.

4.4 RALIS in A Hyperspherical Feature Space

In this section, we look at the geometric properties of RALIS’s components and their compatibility in a hyperspherical latent space.

In contrastive learning, cosine similarity is the most common similarity measure [12]. This approach is often viewed as learning features within a hyperspherical space [37]. By using cosine similarity, contrastive learning encodes information in the angular relationships among vectors while ignoring their magnitudes.

Attention-based view fusion also works well in a hyperspherical space. Views are fused using a weighted sum. When a view weight is applied to a vector, it changes the magnitude of this vector. The fusion will be shifted closer in angle to the longer constituent vectors. If feature vectors are placed into a hyperspherical space, the attention module does not need to account for differences in initial magnitudes. Figure 4 illustrates how two views in a hyperspherical latent space are fused without and with weights; the same principle applies to fusion of more than two views.

We train the MoE classification head using the fused view and all individual views. Since any combination of views resides within the hyperspherical convex hull defined by the individual views (Figure 2), this training strategy equips the gate and the expert models to be more robust to arbitrary, unseen view combinations.

Although the model can still operate with features in a Euclidean space, we project all representations onto a hyperspherical space to ensure consistency across its components. The magnitude normalization below places feature vectors across all views onto a hypersphere. The square root of the vector dimension ensures the feature scale is independent of dimension, preventing excessively small scales for high-dimensional vectors.

$$\text{MagNorm}(z) = \frac{z}{\|z\|} \cdot \sqrt{\dim(z)} \quad (13)$$

Dataset	No. subjects train/ valid/ test	No. views	No. classes
CMDFall	25 / 5 / 20	accel. $\times 2$; 3D pose $\times 5$	20
Daily Sport	3 / 2 / 3	accel. $\times 5$	19
RealDisp	7 / 3 / 7	accel. $\times 9$	33
UP-Fall	7 / 3 / 7	accel. $\times 4$; 2D pose $\times 1$	11

Table 1: Datasets used in experiments.

5 Experiment

5.1 Experimental Setup

5.1.1 Datasets

We use four datasets: CMDFall [42], Daily and Sport Activities [43], UP-Fall [44], and RealDisp [45]. They were chosen for data quantity and diversity, number of views, and annotation granularity. For example, in CMDFall, activities are performed continuously, promoting natural and diverse movements; RealDisp has many sensors and classes. All datasets comprise complex human activities, providing greater discriminative power for robust model evaluation.

Each dataset is divided by subject IDs into training, validation, and test sets. Table 1 summarizes dataset information. For fairness, we use the same labeled training set for all methods in the comparison, including methods using self-supervised contrastive loss. F1-score is used as the evaluation metric to address class imbalance in the test sets.

We use sliding window to create data samples from the raw time series. For all datasets except DailySport, we use a window size of 4 seconds, which is sufficient to capture activities in the label lists. For the DailySport dataset, raw data are originally formatted as 5-second windows.

5.1.2 Baselines

The following methods are included in the comparison: CMC [10], COCOA [20], Flex-MoE [5], FuseMoE [4], and ShaSpec [7]. CMC and COCOA are not explicitly designed for missing views, but since they use contrastive learning and process views independently, the same missing view handling strategy as in RALIS can be applied (Figure 2); these methods are marked with an asterisk in the result tables. Flex-MoE and FuseMoE both use learnable embeddings as missing view indicators and employ MoE to accommodate arbitrary view combinations. ShaSpec learns separate representations for view-specific and shared information; any missing view is reconstructed from the shared features of the available views.

5.1.3 Configurations

For all experiments and methods, we implement a lightweight 1D CNN based on ResNet [46] with 4 residual blocks as the encoder network. Scaling and time warping augmentation techniques [47] are applied to training data. Additionally, 3D rotation is used for accelerometer data, rotation around the Z-axis is applied to 3D poses, and horizontal flipping is applied to 2D

Hyperparameter	Value
optimizer	Adam
learning rate	10^{-3}
classification batch size	16
contrastive learning batch size	16
classification loss weight	1
contrastive loss weight	1
load balancing loss weight	10^{-2}
temperature τ in contrastive loss	0.1
number of experts	16
top K experts	3

Table 2: Hyperparameters for RALIS

poses. Every model is trained for at least 20 epochs, and the best model checkpoint, determined using the validation set, is evaluated on the test set. The batch size is tuned between 8, 16, and 32, and the learning rate is tuned between 10^{-3} , 10^{-4} , and 10^{-5} . For the proposed method, we tune the number of experts between 8, 16, and 32, and top K between 2, 3, and 4. The final hyperparameters of our method are shown in Table 2. All reported scores are averages of three runs with three fixed random seeds.

5.2 Experimental Results

5.2.1 Complete Training Data

We train the models on training sets with complete views and evaluate them on test sets with missing views to assess how they respond to unseen view combinations. For the CMDFall dataset, we use only 3 out of 7 views (1 skeleton and 2 accelerometer views), retaining only samples with all 3 views present. We do not use all 7 views as most samples in this dataset have missing views, hence it is not suitable for this experiment. For each dataset, we evaluate the models under three scenarios: using a single view, half of the views, and all views. For each scenario, the test score is the average across all possible combinations of the specified number of views.

Table 3 shows that our proposed method achieves the highest scores in 10 out of 12 tests. Methods that rely on missing view indicators (i.e., Flex-MoE and FuseMoE) exhibit reduced performance when evaluated on unseen view combinations, particularly in datasets with a large number of views, due to insufficient training of the indicator embeddings for those combinations.

5.2.2 Missing Training Data

To simulate missing views, we randomly drop each view in every sample with a probability of $\sqrt{10^{-3}}$, where V is the number of views, thus each sample has a 0.1% chance of having all views dropped. Except for CMDFall, we use all 7 views without dropping data. The evaluation scenarios are the same as in the previous experiment. Due to missing views, the specified numbers of views now represent upper bounds instead of fixed quantities.

Table 4 shows that RALIS achieves the highest scores overall. The performance gap between RALIS and other methods becomes more pronounced, particularly on the DailySport and RealDisp datasets. This demonstrates RALIS’s robustness to missing views compared to the baselines.

5.3 Ablation Study

We remove each component to assess its contribution to the whole model. Specifically, we examine the following model variants: (1) without the MoE module, (2) without the contrastive loss, (3) without the attention module, (4) without the magnitude norm, (5) without classification training on individual views, (6) without separate load balancing losses for individual views and the fusion, (7) without the stop gradient function before attention, and (8) with full graph instead of adjusted center contrastive loss.

Table 5 presents the results. The poorest results are observed in the variant without individual view training, for which the performance drop is more serious in scenarios with fewer views. The model remains effective when features without magnitude normalization are in a Euclidean space, yielding scores comparable to the proposed version on the RealDisp dataset. Nonetheless, the proposed model still performs better overall compared to this variant.

5.4 More Results with Random View Missing Rate

We conduct another experiment simulating missing views differently. Instead of using a common dropping rate for all views within each dataset, we assign a random dropping rate to each view. Because the missing views of the CMDFall dataset are not simulated, we do not include it in this experiment. Specifically, the dropping rates for views in each dataset are:

- Daily Sport: {"torso": 0.64, "right arm": 0.62, "left arm": 0.77, "right leg": 0.24, "left leg": 0.61}
- RealDisp: {"right lower arm": 0.5, "right upper arm": 0.54, "back": 0.51, "left upper arm": 0.78, "left lower arm": 0.57, "right calf": 0.54, "right thigh": 0.37, "left thigh": 0.53, "left calf": 0.48}
- UP-Fall: {"ankle": 0.49, "belt": 0.34, "neck": 0.24, "wrist": 0.63, "2D pose": 0.69}

Table 6 shows the results for the baseline models, ablation study, and our proposed model. Overall, RALIS achieves the best scores. With a different view missing pattern, these results still remain consistent with the previous experiments.

6 Other Analyses

6.1 Sensitivity Analysis

We perform a sensitivity analysis to evaluate how varying the number of top-K experts and the total number of experts influences model performance. Specifically, we fix the number of top-K experts as specified in Table 2 while varying the total

Dataset No. views	CMDFall			DailySport			RealDisp			UP-Fall		
	1	2	3	1	3	5	1	5	9	1	3	5
CMC*	59.59±0.2	70.80±0.6	76.93±0.9	77.09±1.3	87.03±1.5	92.05±1.6	75.79±1.2	95.06±0.4	97.32±0.1	71.17±0.6	87.31±0.1	91.63±0.5
COCOA*	56.33±0.6	69.29±0.4	76.40±0.6	75.26±0.6	86.31±1.0	90.68±1.4	68.66±0.5	94.55±0.2	97.42±0.2	71.43±0.5	87.24±0.8	91.50±1.6
FlexMoE	25.09±3.8	52.37±2.3	74.42±0.5	12.13±2.3	58.52±4.6	88.40±1.4	03.46±1.6	74.44±2.0	96.92±0.3	09.09±1.3	35.83±4.5	87.14±1.1
FuseMoE	28.49±1.1	55.08±0.6	74.23±1.0	24.21±2.7	70.68±2.1	90.13±0.8	04.31±1.4	65.14±5.7	96.69±0.5	15.07±0.6	62.52±0.9	87.17±0.5
ShaSpec	35.65±0.1	60.59±0.7	74.55±0.5	35.42±1.6	74.46±0.7	88.58±1.5	20.11±4.7	90.14±1.4	97.53±0.5	47.01±2.2	75.62±2.3	90.88±0.5
RALIS	59.95±0.4	71.21±1.1	77.28±1.2	80.56±0.6	90.54±0.7	93.64±0.4	80.75±0.1	95.55±0.1	96.74±0.2	72.75±0.5	86.29±0.3	92.17±0.3

Table 3: F1-score (%) comparison when the training set has complete views.

Dataset No. views	CMDFall			DailySport			RealDisp			UP-Fall		
	1	≤ 4	≤ 7	1	≤ 3	≤ 5	1	≤ 5	≤ 9	1	≤ 3	≤ 5
CMC*	49.41±0.7	74.27±0.3	81.86±0.4	74.24±0.6	82.72±0.6	87.69±0.2	68.86±0.3	84.80±0.3	91.55±0.3	70.84±0.9	82.45±1.1	87.44±0.9
COCOA*	45.71±0.7	71.36±0.5	79.84±0.3	70.98±0.1	81.54±0.3	87.04±0.5	61.61±0.7	82.60±0.4	90.95±0.1	70.12±0.6	83.12±0.7	88.68±1.1
FlexMoE	12.30±0.9	46.04±1.2	74.19±0.6	40.68±2.9	73.72±0.9	86.71±0.9	13.69±0.6	50.17±0.6	70.24±0.6	54.42±2.4	78.22±0.4	87.81±0.5
FuseMoE	09.60±0.7	47.65±1.2	76.22±0.9	49.06±2.6	76.46±1.9	87.62±2.1	28.25±0.9	67.87±0.3	84.35±0.5	52.10±1.8	78.17±0.5	88.69±0.8
ShaSpec	24.61±1.1	61.10±0.5	77.73±0.1	61.77±0.5	78.63±0.5	87.25±0.3	47.76±2.1	78.28±1.2	89.37±0.9	61.59±3.3	80.20±1.8	88.16±1.1
RALIS	50.29±0.4	74.78±0.6	81.75±0.6	79.68±0.3	87.26±0.5	91.25±0.5	76.33±0.1	88.18±0.2	93.33±0.1	74.98±0.5	85.31±0.5	89.72±0.2

Table 4: F1-score (%) comparison when the training set has missing views.

Dataset No. views	CMDFall			DailySport			RealDisp			UP-Fall		
	1	≤ 4	≤ 7	1	≤ 3	≤ 5	1	≤ 5	≤ 9	1	≤ 3	≤ 5
-MoE	49.88±0.4	72.59±0.3	79.29±0.1	77.56±0.9	84.68±0.5	88.49±0.8	75.44±0.4	87.29±0.3	92.04±0.5	73.87±0.9	83.65±0.1	88.73±0.3
-contrast	49.39±0.0	73.97±0.1	81.71±0.4	74.75±0.7	83.61±0.6	88.55±1.3	72.94±0.1	87.09±0.2	92.90±0.2	73.27±0.8	84.34±0.1	90.10±0.2
-attention	49.65±0.6	74.26±0.2	81.54±0.3	78.26±1.5	85.01±1.3	88.60±1.1	76.10±0.3	87.26±0.4	91.53±0.5	74.18±0.7	84.19±0.2	88.86±0.7
-mag. norm	49.25±0.9	73.64±0.8	80.23±0.6	79.56±0.4	86.54±0.1	89.82±0.2	76.13±0.4	88.40±0.3	93.57±0.3	73.82±1.0	84.17±0.8	89.17±1.0
-ind. view	45.85±0.7	71.78±0.3	80.40±0.4	73.12±1.1	83.15±0.3	88.73±0.6	57.81±0.2	79.49±0.3	88.69±0.4	67.81±0.4	81.98±0.4	87.82±0.7
-sep. load	49.36±0.5	73.82±0.8	81.41±0.5	79.28±0.7	86.29±0.8	90.20±0.9	76.06±0.2	88.14±0.2	93.18±0.3	74.82±0.6	84.26±0.3	88.96±0.2
-stop grad	49.75±0.4	74.10±0.1	81.24±0.4	78.34±2.2	86.10±1.0	89.92±1.0	76.14±0.2	88.20±0.3	93.21±0.3	73.58±1.0	83.07±0.4	88.09±0.7
+ full graph	49.68±0.5	74.21±0.5	81.57±0.8	78.50±1.3	85.27±1.5	88.72±1.6	75.52±0.3	87.43±0.0	92.47±0.2	73.78±0.2	83.88±0.2	88.35±0.6
RALIS	50.29±0.4	74.78±0.6	81.75±0.6	79.68±0.3	87.26±0.5	91.25±0.5	76.33±0.1	88.18±0.2	93.33±0.1	74.98±0.5	85.31±0.5	89.72±0.2

Table 5: Ablation study experimental results. For generality, models are trained on data with missing views.

Dataset No. views	DailySport			RealDisp			UP-Fall		
	1	≤ 3	≤ 5	1	≤ 5	≤ 9	1	≤ 3	≤ 5
CMC*	73.66±0.8	80.81±0.8	85.66±1.3	66.41±0.8	80.81±0.4	88.46±0.3	70.25±0.4	77.00±0.6	81.53±0.9
COCOA*	70.27±2.4	78.50±2.6	84.23±2.5	59.72±0.3	77.52±0.1	86.48±0.0	59.80±0.8	68.16±0.6	73.19±0.9
FlexMoE	62.42±0.1	75.94±0.1	83.62±0.1	16.71±0.1	48.63±0.2	65.72±0.2	57.54±1.8	75.11±1.2	84.19±0.8
FuseMoE	60.65±4.0	75.62±1.6	83.97±0.7	27.20±1.7	61.78±1.3	78.56±1.3	56.66±0.5	74.83±0.7	83.97±1.0
ShaSpec	62.37±0.7	74.17±1.1	81.51±2.1	52.61±0.6	76.07±0.1	87.23±0.5	62.98±1.1	77.25±0.6	85.43±0.5
-MoE	75.47±0.9	82.00±0.3	86.00±0.1	72.39±0.0	82.56±0.3	88.14±0.8	66.09±0.4	72.98±0.6	77.45±0.9
-contrast	71.64±1.1	79.38±0.4	83.99±0.2	70.30±0.6	83.17±0.5	89.38±0.8	70.34±1.1	79.78±0.3	85.20±0.4
-attention	75.44±2.5	82.42±1.9	86.60±1.5	73.34±0.1	83.32±0.4	88.54±0.7	72.97±0.5	80.07±0.0	85.10±0.4
-mag. norm	73.14±0.5	81.56±0.2	86.90±0.1	73.94±0.3	84.84±0.3	90.22±0.3	72.69±0.3	80.19±0.5	84.42±0.6
-ind. view	71.92±1.3	81.03±1.3	85.97±1.4	53.89±0.1	74.35±0.1	84.49±0.1	70.47±0.6	78.50±0.7	83.74±0.5
-sep. load	76.36±2.1	83.44±1.3	87.52±0.8	73.52±0.2	84.18±0.0	89.97±0.1	74.29±0.3	80.80±0.0	85.06±0.2
-stop grad	75.47±1.0	82.44±0.8	86.75±1.7	72.92±0.2	83.92±0.0	89.45±0.0	73.86±0.5	80.87±0.7	85.56±0.0
+full graph	73.70±0.7	80.97±0.6	85.97±0.8	73.65±0.4	84.46±0.0	89.91±0.1	72.86±0.1	79.88±0.1	84.03±0.0
RALIS	77.40±0.6	83.55±0.4	87.57±0.7	73.66±0.3	84.78±0.4	90.82±0.6	74.18±0.1	81.33±0.2	86.44±0.5

Table 6: F1-score (%) comparison with random data missing rates.

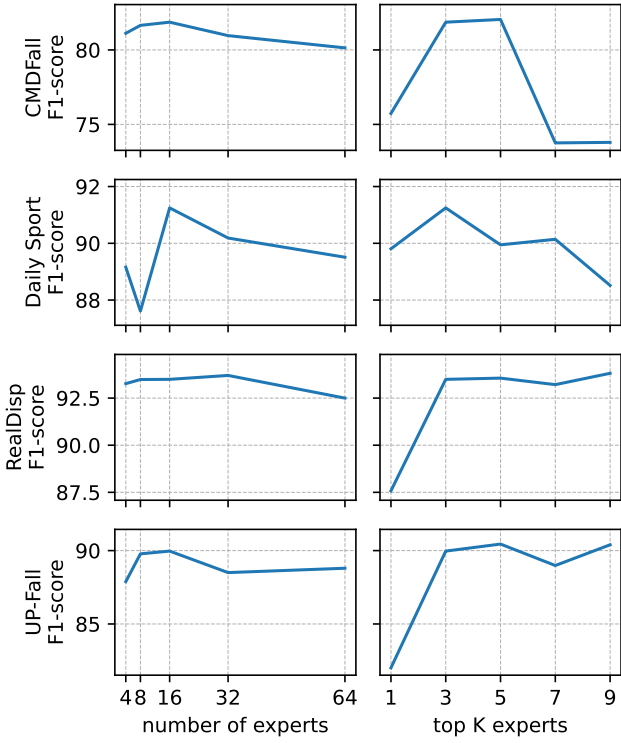


Figure 5: F1-score with varying number of experts and top K experts.

number of experts, and vice versa. Figure 5 shows that using 16 experts yields the best results overall, while increasing the number of experts beyond this point degrades performance in most cases. Regarding top-K selection, the first two datasets experience performance drops as K increases, whereas for the last two datasets, the F1-score remains approximately the same as K increases. Choosing K=3 provides a good balance between accuracy and efficiency.

6.2 Interaction Between Contrastive Loss and Attention Weights

The attention module looks at angular differences in feature vectors to assign weights to the views. Meanwhile, the contrastive loss aligns all views, making it harder for the attention module to distinguish among them. Figure 6 illustrates how contrastive loss and view weights evolve over training epochs. As the contrastive loss decreases, the view weights tend to converge toward a similar level. By influencing the upstream encoders, the contrastive loss indirectly impacts the attention module, even though this module is trained exclusively using the classification loss. This behavior confirms that the contrastive loss is functioning as intended, pulling individual views closer to the fusion. In the model without contrastive loss, view weights do not converge or converge more slowly. Models trained with contrastive loss achieve better overall alignment and accuracy (Table 5), highlighting the efficacy of the proposed method.

6.3 Effects of Separate Load Balancing Loss

As individual views and the fusion are trained jointly, computing the load balancing loss separately for one-view and multi-view combinations helps distribute tokens more evenly among the experts. This prevents disjoint sets of experts from forming between one-view and multi-view combinations, especially when the contrastive loss is insufficient to align them. To visualize this effect more clearly, we reduced the contrastive loss weight to 0.1 and increased the load balancing loss weight to 1 (from the base hyperparameters in Table 2). Each model in this analysis is trained for 10 epochs on the DailySport dataset, with data dropped to simulate missing views. Figure 7 shows the distribution of gating scores among 16 experts for one-view and multi-view combinations, both with and without the separate load balancing strategy. The gate trained with the separate load balancing loss exhibits more similar distributions between one-view and multi-view combinations, thus achieving the intended effect.

6.4 Time Complexity Analysis

We empirically compare the time complexity of three contrastive loss functions by measuring the runtime across varying numbers of views and batch sizes, assessing whether observed runtimes align with theoretical complexity. Specifically, we compare the full graph approach–complexity $O(V^2N^2)$ [10], the COCOA loss– $O(V^2N+VN^2)$ [20], and our adjusted center contrastive loss– $O(VN^2)$. All measurements are conducted on the RealDisp dataset with identical software on the same computer equipped with an Nvidia Quadro RTX4000 GPU and an Intel Xeon Gold 6140 CPU. For each method, we record both the loss computation time and the optimization time per batch, averaging results over 450 consecutive batches. Figure 8 presents the results across a range of view counts and batch sizes. As the number of views increases, the runtimes of COCOA loss and adjusted center contrastive loss scale similarly, while the full graph loss exhibits a substantially steeper increase. With larger batch sizes, the adjusted center loss remains the most efficient, whereas the other two methods show comparable scaling. These empirical results are consistent with theoretical expectations. For optimization time, all methods behave similarly except for the full graph loss, which becomes increasingly costly as the number of views grows.

7 Conclusion

This paper introduces RALIS for flexible multimodal multi-view HAR. RALIS can handle arbitrarily missing views during both training and inference, while avoiding redundant missing view reconstruction.

The model is trained with a load balancing loss for MoE, an adjusted center contrastive loss, and a classification loss. It leverages both labeled and unlabeled data since contrastive loss does not require labels. Contrastive learning maximizes mutual information among views by aligning different views of the same sample, mitigating the impact of missing views.

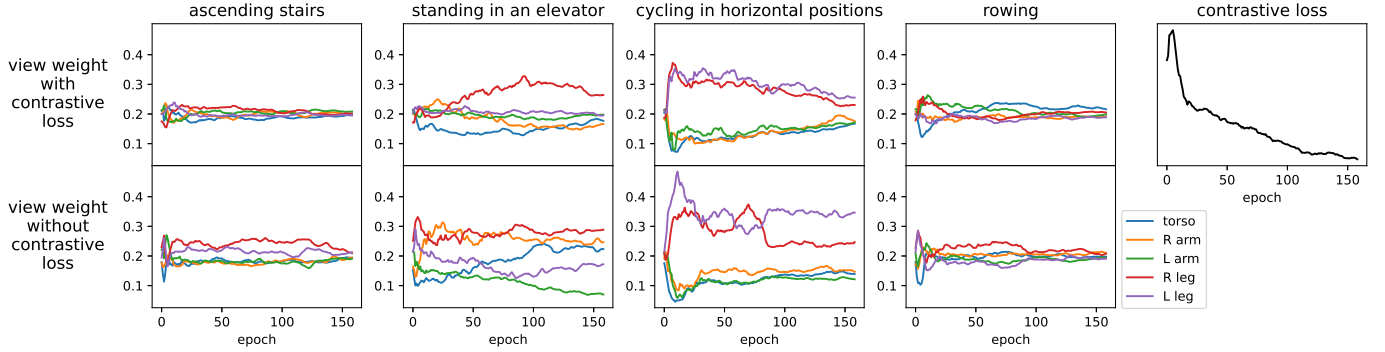


Figure 6: View weights for several classes and contrastive loss over training epochs on the Daily and Sport Activities dataset.

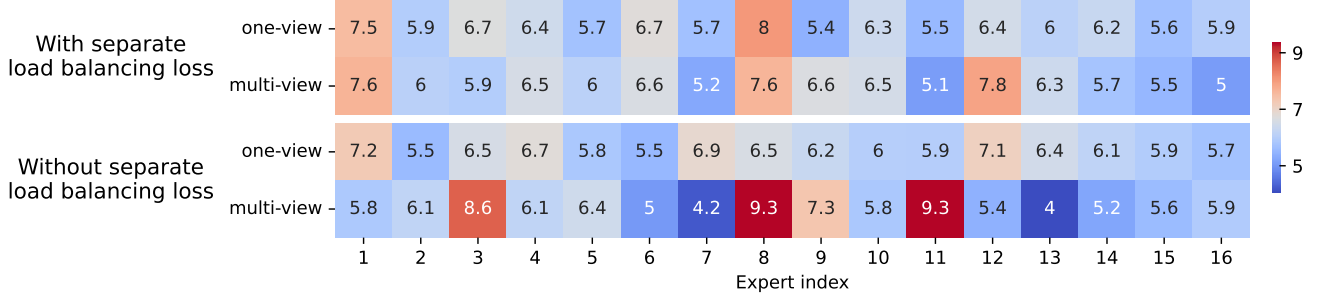


Figure 7: Distribution of gating scores among 16 experts for one-view and multi-view combinations, comparing training with and without separate load balancing loss. Each row is normalized to sum to 100.

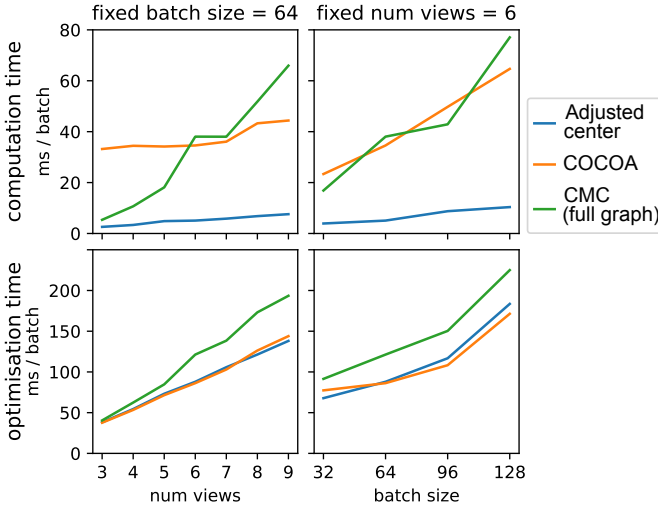


Figure 8: Runtime of contrastive loss methods across varying numbers of views and batch sizes.

An attention module assigns view weights, dynamically adjusting view fusion for both contrastive learning and classification. The MoE head addresses residual discrepancies among view combinations that arise from view-specific features and are not captured by contrastive learning.

In HAR, different views often share information as the person’s body moves. In rare cases when views share minimal mutual information, contrastive learning’s effectiveness would be limited. Our approach samples negative pairs for contrastive

loss within each batch, which is effective when the data are diverse. This may be less effective when samples are highly similar, as often seen in modalities like electrocardiography or electroencephalography. These issues need to be addressed when adapting the proposed method to other fields besides HAR.

Our method processes views separately to accommodate missing data. While it retains useful view-specific features, it does not model cross-view interactions, except at the fusion step. Although experiments show it performs favorably compared to methods incorporating cross-view interactions (e.g., using Transformer), this remains an avenue for future exploration, particularly in scenarios with missing views.

References

- [1] Duc-Anh Nguyen and Nhien-An Le-Khac. Sok: Behind the accuracy of complex human activity recognition using deep learning. In *2024 International Joint Conference on Neural Networks (IJCNN)*, pages 1–8, 2024.
- [2] YongKyung Oh and Sungil Kim. Multi-modal lifelog data fusion for improved human activity recognition: A hybrid approach. *Information Fusion*, 110:102464, October 2024.
- [3] Antonio A. Aguileta, Ramon F. Brena, Oscar Mayora, Erik Molino-Minero-Re, and Luis A. Trejo. Multi-sensor fusion for activity recognition—a survey. *Sensors*, 19(17), 2019.
- [4] Xing Han, Huy Nguyen, Carl William Harris, Nhat Ho,

and Suchi Saria. Fusemoe: Mixture-of-experts transformers for fleximodal fusion. In *The Thirty-eighth Annual Conference on Neural Information Processing Systems*, 2024.

[5] Sukwon Yun, Inyoung Choi, Jie Peng, Yangfan Wu, Jingxuan Bao, Qiyiwen Zhang, Jiayi Xin, Qi Long, and Tianlong Chen. Flex-moe: Modeling arbitrary modality combination via the flexible mixture-of-experts. In *The Thirty-eighth Annual Conference on Neural Information Processing Systems*, 2024.

[6] Sangmin Woo, Sumin Lee, Yeonju Park, Muhammad Adi Nugroho, and Changick Kim. Towards good practices for missing modality robust action recognition. *Proceedings of the AAAI Conference on Artificial Intelligence*, 37(3):2776–2784, Jun. 2023.

[7] Hu Wang, Yuanhong Chen, Congbo Ma, Jodie Avery, Louise Hull, and Gustavo Carneiro. Multi-modal learning with missing modality via shared-specific feature modelling. In *Proceedings of the IEEE/CVF Conference on Computer Vision and Pattern Recognition (CVPR)*, pages 15878–15887, June 2023.

[8] Rui Liu, Haolin Zuo, Zheng Lian, Björn W. Schuller, and Haizhou Li. Contrastive learning based modality-invariant feature acquisition for robust multimodal emotion recognition with missing modalities. *IEEE Transactions on Affective Computing*, 15(4):1856–1873, October 2024.

[9] Songtao Li and Hao Tang. Multimodal alignment and fusion: A survey, 2024.

[10] Yonglong Tian, Dilip Krishnan, and Phillip Isola. Contrastive multiview coding. In Andrea Vedaldi, Horst Bischof, Thomas Brox, and Jan-Michael Frahm, editors, *Computer Vision – ECCV 2020*, pages 776–794, Cham, 2020. Springer International Publishing.

[11] Zihao Chen, Chi-Heng Lin, Ran Liu, Jingyun Xiao, and Eva L. Dyer. Your contrastive learning problem is secretly a distribution alignment problem. In A. Globerson, L. Mackey, D. Belgrave, A. Fan, U. Paquet, J. Tomczak, and C. Zhang, editors, *Advances in Neural Information Processing Systems*, volume 37, pages 91597–91617. Curran Associates, Inc., 2024.

[12] Hui Chen, Charles Gouin-Vallerand, Kévin Bouchard, Sébastien Gaboury, Mélanie Couture, Nathalie Bier, and Sylvain Giroux. Contrastive self-supervised learning for sensor-based human activity recognition: A review. *IEEE Access*, 12:152511–152531, 2024.

[13] Philip Bachman, R Devon Hjelm, and William Buchwalter. Learning representations by maximizing mutual information across views. In *Advances in Neural Information Processing Systems*, volume 32. Curran Associates, Inc., 2019.

[14] Jie Xu, Shuo Chen, Yazhou Ren, Xiaoshuang Shi, Hengtao Shen, Gang Niu, and Xiaofeng Zhu. Self-weighted contrastive learning among multiple views for mitigating representation degeneration. In A. Oh, T. Naumann, A. Globerson, K. Saenko, M. Hardt, and S. Levine, editors, *Advances in Neural Information Processing Systems*, volume 36, pages 1119–1131. Curran Associates, Inc., 2023.

[15] Noam Shazeer, *Azalia Mirhoseini, *Krzysztof Maziarz, Andy Davis, Quoc Le, Geoffrey Hinton, and Jeff Dean. Outrageously large neural networks: The sparsely-gated mixture-of-experts layer. In *International Conference on Learning Representations*, 2017.

[16] Cunling Bian, Wei Feng, Fanbo Meng, and Song Wang. Global-local contrastive multiview representation learning for skeleton-based action recognition. *Computer Vision and Image Understanding*, 229:103655, March 2023.

[17] Jie Xu, Huayi Tang, Yazhou Ren, Liang Peng, Xiaofeng Zhu, and Lifang He. Multi-level feature learning for contrastive multi-view clustering. In *Proceedings of the IEEE/CVF Conference on Computer Vision and Pattern Recognition (CVPR)*, pages 16051–16060, June 2022.

[18] Shuvendu Roy and Ali Etemad. Self-supervised contrastive learning of multi-view facial expressions. In *Proceedings of the 2021 International Conference on Multi-modal Interaction*, ICMI ’21, page 253–257, New York, NY, USA, 2021. Association for Computing Machinery.

[19] Yijie Lin, Yuanbiao Gou, Xiaotian Liu, Jinfeng Bai, Jiancheng Lv, and Xi Peng. Dual contrastive prediction for incomplete multi-view representation learning. *IEEE Transactions on Pattern Analysis and Machine Intelligence*, 45(4):4447–4461, 2023.

[20] Shohreh Deldari, Hao Xue, Aaqib Saeed, Daniel V. Smith, and Flora D. Salim. Cocoa: Cross modality contrastive learning for sensor data. *Proc. ACM Interact. Mob. Wearable Ubiquitous Technol.*, 6(3), September 2022.

[21] Guanzhou Ke, Zhiyong Hong, Zhiqiang Zeng, Zeyi Liu, Yangjie Sun, and Yannan Xie. Conan: Contrastive fusion networks for multi-view clustering. In *2021 IEEE International Conference on Big Data (Big Data)*, page 653–660. IEEE, December 2021.

[22] Song Wu, Yan Zheng, Yazhou Ren, Jing He, Xiaorong Pu, Shudong Huang, Zhifeng Hao, and Lifang He. Self-weighted contrastive fusion for deep multi-view clustering. *IEEE Transactions on Multimedia*, 26:9150–9162, 2024.

[23] Guanghui Zhu, Wang Lu, Chunfeng Yuan, and Yihua Huang. Adamcl: Adaptive fusion multi-view contrastive learning for collaborative filtering. In *Proceedings of the*

46th International ACM SIGIR Conference on Research and Development in Information Retrieval, SIGIR '23, page 1076–1085. ACM, July 2023.

[24] Yash Jain, Chi Ian Tang, Chulhong Min, Fahim Kawsar, and Akhil Mathur. Collossl: Collaborative self-supervised learning for human activity recognition. *Proc. ACM Interact. Mob. Wearable Ubiquitous Technol.*, 6(1), March 2022.

[25] William Fedus, Jeff Dean, and Barret Zoph. A review of sparse expert models in deep learning, 2022.

[26] Weilin Cai, Juyong Jiang, Fan Wang, Jing Tang, Sunghun Kim, and Jiayi Huang. A survey on mixture of experts in large language models. *IEEE Transactions on Knowledge and Data Engineering*, page 1–20, 2025.

[27] Basil Mustafa, Carlos Riquelme, Joan Puigcerver, Rodolphe Jenatton, and Neil Houlsby. Multimodal contrastive learning with limoe: the language-image mixture of experts. In S. Koyejo, S. Mohamed, A. Agarwal, D. Belgrave, K. Cho, and A. Oh, editors, *Advances in Neural Information Processing Systems*, volume 35, pages 9564–9576. Curran Associates, Inc., 2022.

[28] Tongxu Luo, Jiahe Lei, Fangyu Lei, Weihao Liu, Shizhu He, Jun Zhao, and Kang Liu. Moelora: Contrastive learning guided mixture of experts on parameter-efficient fine-tuning for large language models, 2024.

[29] Yunhe Zhang, Jinyu Cai, Zhihao Wu, Pengyang Wang, and See-Kiong Ng. Mixture of experts as representation learner for deep multi-view clustering. *Proceedings of the AAAI Conference on Artificial Intelligence*, 39(21):22704–22713, Apr. 2025.

[30] Siyu Liu, Haoran Wang, Shiman Li, and Chenxi Zhang. Mixture-of-experts and semantic-guided network for brain tumor segmentation with missing mri modalities. *Medical & Biological Engineering & Computing*, 62(10):3179–3191, May 2024.

[31] Anil Rahate, Rahee Walambe, Sheela Ramanna, and Ketan Kotecha. Multimodal co-learning: Challenges, applications with datasets, recent advances and future directions. *Information Fusion*, 81:203–239, 2022.

[32] Duc-Anh Nguyen, Cuong Pham, and Nhien-An Le-Khac. Virtual fusion with contrastive learning for single-sensor-based activity recognition. *IEEE Sensors Journal*, 24(15):25041–25048, 2024.

[33] Wei Luo, Mengying Xu, and Hanjiang Lai. *Multimodal Reconstruct and Align Net for Missing Modality Problem in Sentiment Analysis*, page 411–422. Springer Nature Switzerland, 2023.

[34] Yixuan Wu, Jintai Chen, Lianting Hu, Hongxia Xu, Huiying Liang, and Jian Wu. Omnifuse: A general modality fusion framework for multi-modality learning on low-quality medical data. *Information Fusion*, 117:102890, May 2025.

[35] Jack Geraghty, Andrew Hines, and Fatemeh Golpayegani. Learning to associate: Multimodal inference with fully missing modalities. *ACM Transactions on Intelligent Systems and Technology*, June 2025.

[36] Renjie Wu, Hu Wang, Hsiang-Ting Chen, and Gustavo Carneiro. Deep multimodal learning with missing modality: A survey, 2024.

[37] Tongzhou Wang and Phillip Isola. Understanding contrastive representation learning through alignment and uniformity on the hypersphere. In Hal Daumé III and Aarti Singh, editors, *Proceedings of the 37th International Conference on Machine Learning*, volume 119 of *Proceedings of Machine Learning Research*, pages 9929–9939. PMLR, 13–18 Jul 2020.

[38] Ziyu Liu, Azadeh Alavi, Minyi Li, and Xiang Zhang. Self-supervised contrastive learning for medical time series: A systematic review. *Sensors*, 23(9):4221, April 2023.

[39] Ye Yuan, Guangxu Xun, Fenglong Ma, Yaqing Wang, Nan Du, Kebin Jia, Lu Su, and Aidong Zhang. Muvan: A multi-view attention network for multivariate temporal data. In *2018 IEEE International Conference on Data Mining (ICDM)*, page 717–726. IEEE, November 2018.

[40] HaoJie Ma, Wenzhong Li, Xiao Zhang, Songcheng Gao, and Sanglu Lu. Attnsense: Multi-level attention mechanism for multimodal human activity recognition. In *Proceedings of the Twenty-Eighth International Joint Conference on Artificial Intelligence, IJCAI-19*, pages 3109–3115. International Joint Conferences on Artificial Intelligence Organization, 7 2019.

[41] Bo Yang, Sen Wang, Andrew Markham, and Niki Trigoni. Robust attentional aggregation of deep feature sets for multi-view 3d reconstruction. *International Journal of Computer Vision*, 128(1):53–73, Jan 2020.

[42] Thanh-Hai Tran, Thi-Lan Le, Dinh-Tan Pham, Van-Nam Hoang, Van-Minh Khong, Quoc-Toan Tran, Thai-Son Nguyen, and Cuong Pham. A multi-modal multi-view dataset for human fall analysis and preliminary investigation on modality. In *2018 24th International Conference on Pattern Recognition (ICPR)*, pages 1947–1952, 2018.

[43] Kerem Altun, Billur Barshan, and Orkun Tunçel. Comparative study on classifying human activities with miniature inertial and magnetic sensors. *Pattern Recognition*, 43(10):3605–3620, 2010.

- [44] Lourdes Martínez-Villaseñor, Hiram Ponce, Jorge Brieva, Ernesto Moya-Albor, José Núñez-Martínez, and Carlos Peñafort-Asturiano. Up-fall detection dataset: A multi-modal approach. *Sensors*, 19(9), 2019.
- [45] Oresti Baños, Miguel Damas, Héctor Pomares, Ignacio Rojas, Máté Atila Tóth, and Oliver Amft. A benchmark dataset to evaluate sensor displacement in activity recognition. In *Proceedings of the 2012 ACM Conference on Ubiquitous Computing, UbiComp '12*, page 1026–1035, New York, NY, USA, 2012. Association for Computing Machinery.
- [46] Kaiming He, Xiangyu Zhang, Shaoqing Ren, and Jian Sun. Deep residual learning for image recognition. In *Proceedings of the IEEE Conference on Computer Vision and Pattern Recognition (CVPR)*, June 2016.
- [47] Terry T. Um, Franz M. J. Pfister, Daniel Pichler, Satoshi Endo, Muriel Lang, Sandra Hirche, Urban Fietzek, and Dana Kulić. Data augmentation of wearable sensor data for parkinson's disease monitoring using convolutional neural networks. In *Proceedings of the 19th ACM International Conference on Multimodal Interaction, ICMI '17*, page 216–220, New York, NY, USA, 2017. Association for Computing Machinery.